Mineralogy and Petrology (2018) 112 (Suppl 1):S115–S132
https://doi.org/10.1007/s00710-018-0610-y

ORIGINAL PAPER

The mantle of Scotland viewed through the Glen Gollaidh aillikite

Mark T. Hutchison[1] · John W. Faithfull[2] · Dan N. Barfod[3] · Joshua W. Hughes[4] · Brian G. J. Upton[5]

Received: 15 November 2017 / Accepted: 30 May 2018 / Published online: 11 July 2018

Abstract

The Glen Gollaidh aillikite dyke (58.36741°N 4.69751°W), N.W. Scotland, occurs within the Neoproterozoic sedimentary rocks of the Moine Supergroup ~4 km east of the Moine Thrust. Phlogopite $^{40}Ar/^{36}Ar$ measurements give a late Devonian maximum emplacement age of 360.3 ± 4.9 (2σ) Ma. This age occurs in a quiet period of Scottish magmatic history c. 30 Ma after the closure of the Iapetus and before the start of intra-plate alkali magmatism which affected southern Scotland for ~60 My from c. 350 Ma. Abundant chromites and Cr-diopsides and a few unaltered olivines, reflecting a mantle provenance, were recovered from heavy mineral concentrates. The North Atlantic Craton, exposed in Lewisian gneisses west of the Moine thrust, is therefore inferred to extend east at depth under Glen Gollaidh, presenting an opportunity to investigate the thickness and composition of the cratonic margin in the Devonian. The aillikite was found to be barren of diamond and no picro-ilmenites or garnets were definitively identified. However, mineral chemistry suggests that a proportion of Glen Gollaidh xenocrysts crystallised in equilibrium with garnet. Most spinels are Mg, Al chromites, with some Mg chromite present. All fall within the garnet peridotite field based on Ti and Cr but with insufficient Cr_2O_3 (up to 47.2 wt%) to be consistent with the diamond stability field. Amongst Cr-diopsides 30% of grains have Cr and Al contents consistent with derivation from garnet peridotite. The majority of clinopyroxenes also show a marked depletion in heavy compared to light rare-earth elements, again consistent with equilibration with garnet. The opx-cpx solvus thermometer demonstrates that average Cr-diopside compositions require at least 37 kbar to give a temperature (979 °C) lying even on a relatively warm 40 mWm^{-2} geotherm (Hasterok and Chapman Earth Planet Sc Lett 307:59–70, 2011). Large variations in the chemistry of mantle minerals reflect a complex history of metasomatism akin to constituents of alkali igneous rocks elsewhere in the Hebridean and Northern Highlands Terranes. Fertilised mantle provided the conditions for generation of aillikite melts, probably triggered by break-off of the advancing Avalonia slab. The cratonic root underlying the Glen Gollaidh aillikite during the late Devonian was apparently too thin to lie within the diamond stability field, consistent with xenoliths from alkali basalts further south. Nonetheless, sufficient geophysical and mineral chemical evidence supports Glen Gollaidh aillikite sitting close to the edge of diamond-prospective mantle therefore suggesting diamond potential a short distance to the west within the Lewisian and what is now East Greenland.

Keywords Aillikite · Scotland · North Atlantic Craton · Metasomatism · Cr-diopside · Diamond

Editorial handling: G. Pearson

Electronic supplementary material The online version of this article (https://doi.org/10.1007/s00710-018-0610-y) contains supplementary material, which is available to authorized users.

✉ Mark T. Hutchison
mth@trigon-gs.com

✉ Dan N. Barfod
Dan.Barfod@glasgow.ac.uk

[1] Trigon GeoServices Ltd, #35-15, 2780 South Jones Blvd., Las Vegas, NV 89146, USA

[2] Hunterian Museum, University of Glasgow, Glasgow G12 8QQ, UK

[3] Scottish Universities Environmental Research Centre, Scottish Enterprise Technology Park, East Kilbride G75 0QF, UK

[4] Department of Earth Sciences, University of Durham, Durham DH1 3LE, UK

[5] School of Geosciences, University of Edinburgh, Edinburgh EH9 3FE, UK

Introduction

Smith et al. (2008) and Faithfull (2012) describe a carbonate-rich olivine macrocrystal dyke in Sutherland, Scotland originally reported as a monchiquite (Read 1931). More recent petrology correctly reclassifies the dyke as an aillikite (Hughes 2012). Aillikites have not otherwise been recorded in the UK and are particularly notable because in some locations they are hosts for diamonds (Hutchison and Frei 2009). As deep-sourced rocks with mantle components aillikites also inform us on the dynamics of the sub-lithospheric mantle which in Scotland likely differs from better exposed rocks sharing a common but more centrally located membership of the North Atlantic Craton (NAC). Here we determine emplacement age and report on the xenocryst component, thus allowing the Glen Gollaidh dyke to provide a time-specific window on the mantle lithosphere comprising the Scottish part of the NAC margin.

Geology

The 1 m wide dyke, named after its location in Glen Gollaidh (also termed Glen Golly), is exposed at 58.36741°N 4.69751°W, to the west of Ben Hope (Fig. 1). Stream-bed outcrops can be seen at two further locations <75 m west northwest along the Allt Strath Feinne-bheinne and a fourth lies 250 m east-southeast along the dyke's ~100° strike within the Alltan Molach (Hughes 2012). Glen Gollaidh is situated within the Northern Highland Terrane amongst Neoproterozoic rocks of the Moine Supergroup. The Lewisian gneisses, the crustal expression of the margin of the North Atlantic Craton (NAC), occur a short distance (~4 km) to the west in the footwall of the Moine Thrust.

The dyke shows considerable internal variability in mineralogy and texture. Despite this, it is consistently porphyritic with larger grains (>3 mm and up to 8 mm) interpreted to be dominantly xenocrysts and smaller grains a mixture of phenocrysts and broken xenocrysts (Fig. 2a). Primary minerals consist of olivine (fresh and serpentinised), calcite, phlogopite (often longer than 1 mm, and with tetraferriphlogopite rims), clinopyroxene (cpx), apatite, chromite, magnetite, and accessory perovskite, rutile, Ca–Ti ± REE and Zr oxides, barite and pyrite. Spinels and perovskites commonly surround larger serpentinised olivines forming a necklace-like texture (Fig. 2b) and individual spinel grains occasionally show atoll-shaped textures typical of kimberlites (Fig. 2a; Mitchell 1986). Mineralogy and bulk chemical analyses (Hughes 2012; Supplementary Table 1) classify the rock as an aillikite (after Rock 1986; Tappe et al. 2005). While the presence of primary groundmass clinopyroxene precludes identification as kimberlite, the two rock-types, aillikite and kimberlite, are closely genetically and mineralogically related. Both generate interest for diamond potential and typically tap considerable depths within the mantle lithosphere. Larger phlogopites are commonly bent (Fig. 2b) implying emplacement as a crystal mush. The dyke grades into carbonatite (>50% carbonate by volume) along strike (Hughes 2012) due to fluctuating compositions being fed into the steadily dilating fissure. Similarly intimate aillikite / carbonatite associations have been documented in the NAC in West Greenland (Hutchison and Frei 2009) and at its southern margin in the Gardar assemblage (Upton et al. 2006) where textures are interpreted to have resulted from flow-differentiation due to the melts being of contrasting ductility (Upton 2013). Bulk rock analysis of the Glen Gollaidh aillikite shows no strong compositional gap along the gradation between aillikite and carbonatite (Supplementary Table 1). Calcite veinlets up to 5 mm thick are particularly common at the northwestern extent of the dyke.

Xenocrysts and clasts consist of olivines and orthopyroxenes (almost exclusively pseudomorphed) and abundant serpentinised spinel lherzolite xenoliths (≤3 cm; Fig. 2c) and reflect a mantle component. Titanian and magnesian magnetites form pronounced reaction rims around isolated grains of brown spinel (Fig. 2a), indicating clearly that spinel-lherzolites have been disaggregated and reacted with the melt. Akin to other aillikites (Hutchison and Frei 2009), smaller olivine grains are expected to be a combination of phenocrysts and broken xenocrysts, emphasising the importance of mineral petrology rather than bulk chemical measurement in determination of the rock type. Weathered surfaces show the very competent, sandpaper-textured orange-brown knobbly appearance (Fig. 2d) ubiquitous in NAC aillikites (Hutchison and Frei 2009).

Samples and methodology

Hand samples were collected for the purposes of determination of emplacement age and characterisation of mantle minerals by means of disaggregation and mineral separation. Weathered surfaces were removed before further sample processing was carried out.

Fig. 1 Simplified geological map of Scotland emphasising the influence of deformation and magmatism arising from the closure of the Iapetus Ocean and associated Caledonian orogeny. Modified from Stephenson (2000). GG (green circle) = location of Glen Gollaidh aillikite. Localities of other notable intrusive igneous rocks (alkali basalts, syenites and lamprophyres) are indicated by red circles: Ss = Sandsting, RNB = Rinibar, LL = Loch Loyal, LB = Loch Borralan (Loch Borolan), LR = Loch Roag, SC = Streap Com'laidh, Sa'G = Stobh a'Ghrianain, GRB = Gribun, HN = Hawk's Nib, HoA = Heads of Ayr, DG = Dunaskin Glen, Cr = Criffel, HEX = Hexpath, WL = Weak Law, FD = Fidra, EN = Elie Ness. Clare Island, Eire, referred to in the text, lies off the western edge of the map at 53°48′ N 9°59′ W in Ireland's North Western Terrane - the equivalent of the Midland Valley Terrane

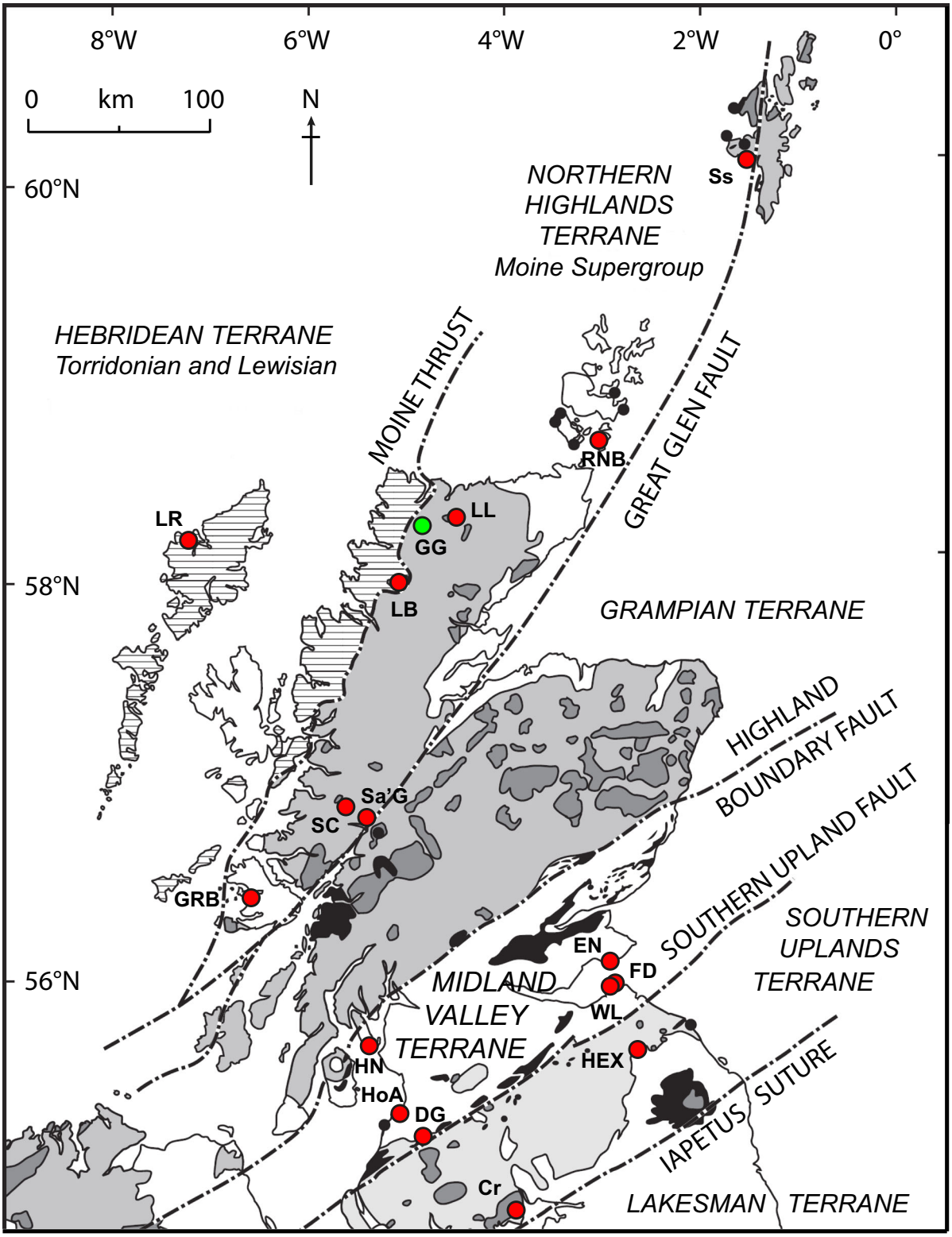
8°W
6°W
4°W
2°W
0°
0 km 100
N
60°N
58°N
56°N
NORTHERN HIGHLANDS TERRANE
Moine Supergroup
HEBRIDEAN TERRANE
Torridonian and Lewisian
MOINE THRUST
GREAT GLEN FAULT
HIGHLAND BOUNDARY FAULT
SOUTHERN UPLAND FAULT
GRAMPIAN TERRANE
SOUTHERN UPLANDS TERRANE
MIDLAND VALLEY TERRANE
IAPETUS SUTURE
LAKESMAN TERRANE
Ss
RNB
LL
GG
LB
LR
Sa'G
SC
GRB
EN
FD
WL
HEX
HN
HoA
DG
Cr
post-Silurian rocks (other than Devonian igneous rocks)
Caledonian volcanics (Ordovician to Devonian (circles - small outcrops)
Caledonian intrusive rocks (Ordovician to Upper Devonian)
Upper Proterozoic rocks affected by Caledonian deformation events
Upper Proterozoic to Silurian rocks affected by late Caledonian deformation (Acadian)
Archean, Proterozoic and lower Paleozoic rocks unaffected by Caledonian deformation

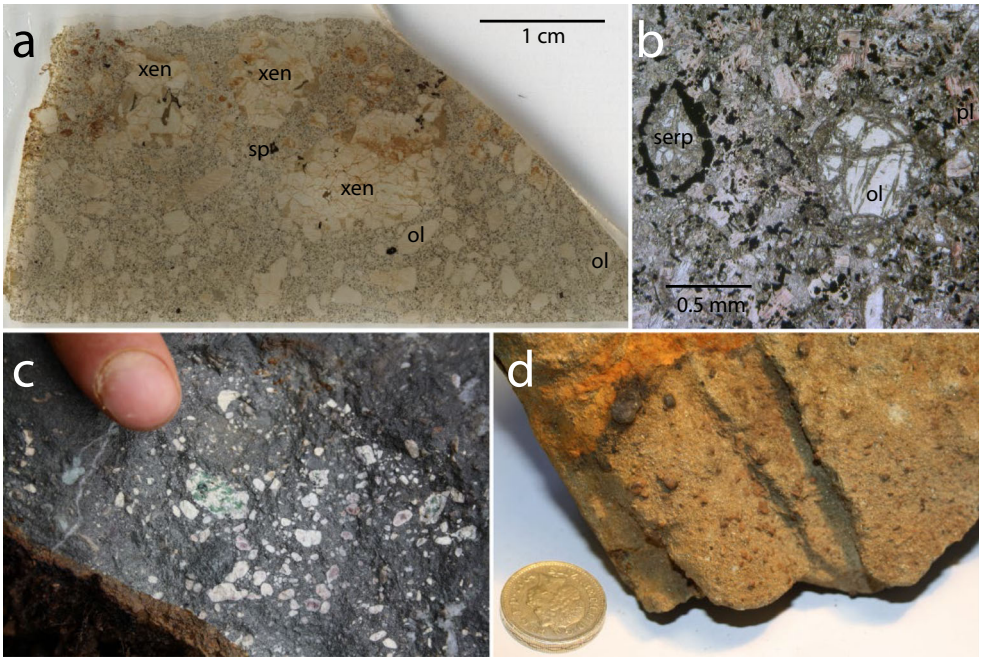

Fig. 2 Samples of typical Glen Gollaidh aillikite. **a** Thin section showing phenocrystic texture with spinel lherzolite xenoliths (xen) and olivine xenocrysts (ol; up to 5 mm). Macrocrysts of spinel (sp; red-brown bordered by opaque chromite and perovskite) are evident. **b** Photomicrograph under plain polarised light showing deformed phlogopites (pl; 0.3 mm brown platy minerals) on the right edge. One large (0.6 mm) olivine macrocryst (ol) lies off centre to the right and another, highly serpentinised (serp) is surrounded by a necklace-texture of opaque chromites and perovskite (square cross-sections). **c** Hand sample of freshly exposed surface showing abundant carbonated olivine xenocrysts and spinel lherzolite xenolith with carbonate veining and segregation textures. The thickness (<5 mm) of the weathered layer is apparent in section. **d** Hand sample of distinctive orange-brown, nodular and sandpaper-textured weathered aillikite. The appearance is characteristic of aillikite and kimberlite samples in the field in the North Atlantic Craton (Hutchison and Frei 2009)

Age determination

Phlogopite was separated from the freshest and coarsest mica-rich material collected, a block of interbanded macrocrystal and carbonate-rich aillikite (sample 43A4). Each analysed aliquot represents 10 grains of phlogopite with an average diameter between 250 and 500 μm. Samples and neutron flux monitors were packaged in copper foil and stacked in quartz tubes with the relative positions of packets precisely measured for later reconstruction of neutron flux gradients. The sample package was irradiated in the Oregon State University reactor, Cd-shielded facility. Fish Canyon sanidine (28.294 ± 0.036 (1σ) Ma, Renne et al. 2011) was used to monitor ^{39}Ar production and establish neutron flux values (J) for the samples. Gas was extracted from samples via step-heating using a mid-infrared (10.6 μm) CO_2 laser with a non-Gaussian, uniform energy profile and a 2.0 mm beam diameter. The samples were housed in a doubly-pumped ZnS-window laser cell and loaded into a stainless steel planchette containing 208 wells of 2 mm diameter. Liberated argon was purified of active gases, e.g., CO_2, H_2O, H_2, N_2, CH_4, using two Zr-Al getters; one at 16 °C and another at 400 °C. Data were collected on a Mass Analyser Products MAP-215-50 single-collector mass spectrometer using an electron multiplier collector in dynamic collection (peak hopping) mode. Time-intensity data are regressed to inlet time with second-order polynomial fits to the data. The average total system blank for laser extractions, measured between each sample run, was $1.2 \pm 0.2 \times 10^{-15}$ mol ^{40}Ar, $4.6 \pm 2.2 \times 10^{-17}$ mol ^{39}Ar, $8.0 \pm 0.9 \times 10^{-18}$ mol ^{36}Ar. Mass discrimination was monitored on a daily basis, between and within sample runs by analysis of an air standard aliquot delivered by an automated pipette system. All blank, interference and mass discrimination calculations were performed with the MassSpec software package (MassSpec, version 8.16, authored by Al Deino, Berkeley Geochronology Center). Inverse-variance-weighted plateau ages, or composite plateau ages for replicated samples, are chosen as the best estimates of the emplacement ages. Plateau ages were defined following these criteria:

1) Steps overlap in age within 2σ uncertainty. 2) Minimum ^{39}Ar content for a step is ≥0.1% by weight of total ^{39}Ar release. 3) Minimum of three contiguous steps. 4) Minimum of 50% by weight of ^{39}Ar in the chosen steps. 5) The inverse isochron formed by the plateau steps yields an age indistinguishable from the plateau age at 2σ uncertainty. 6) The trapped component composition, derived from this inverse

isochron, is indistinguishable from the composition of air at the 2σ uncertainty level. 7) Age and uncertainty (SEM) were calculated using the mean weighted by the inverse variance of each step. 8) For samples with MSWD >95%, the uncertainty is expanded by the square root of MSWD and Student's t. Analytical data and results are presented in Table 1.

Sample processing for mantle mineral chemistry

A 9.8 kg aillikite sample was disaggregated to <1 mm grain size in two batches by high-voltage pulse fragmentation with all fines retained. All 6.05 kg of 0.25–1.0 mm grains, and 500 g of 0.18–0.25 mm grains were liquid density separated (S.G. 2.96) with a purpose-designed flowsheet built to retain any microdiamonds. Mantle-derived minerals were identified by optical microscopy, mounted in epoxy and polished to 0.25 μm for mineral chemical analyses. Subsequently 38 g of sample was archived and the total remaining sample was treated by caustic fusion for identification of diamond down to a threshold of 75 μm.

Mineral chemical determination

All analysed clinopyroxenes and olivines derive from the >250 μm size fraction whereas analysed spinels derive from both 180–250 μm and > 250 μm fractions. Major element chemistry was determined by Cameca SX100 electron probe microanalyser (EPMA; 15 keV, 10 and 100 nA, beam-size 5 μm). All elemental concentrations were determined from measurement of Kα lines with 20 to 60 s counting times on peaks and 10 to 60 s on background positions. Analyses were calibrated using internal well-characterised standards as follows: Al and Mg - Spinel-BL8; Ca and Si - Wollastonite-BL7; Cr - PuCr-BL7; Fe - Fayalite; Mn - PuMn-BL8; Na - Jadeite-BL7; Ni - PuNi-BL8; Ti - Rutile-BL8. Matrix corrections were made by the proprietary PAP software supplied by the manufacturer of the instrument. Spinels were classified by major element chemistry subdivision according to criteria modified from Ramsay (1992) and described in Hutchison (2018).

Determination of accurate concentrations of twenty-seven trace elements were made by laser ablation inductively coupled mass spectrometry (La-ICP-MS) using a Hewlett Packard Agilent 7700 mass spectrometer. The instrument employs an Excimer 193 nm laser and samples and standards were mounted in a custom built, dual volume sample cell. Instrument and data deconvolution methodologies employed follow Norman et al. (1996).

Olivine trace element analyses were performed with a 5 Hz laser repetition rate whereas clinopyroxenes and chromites were analysed at 10 Hz. Olivine and clinopyroxene grains were large enough to be analysed with a beam size of 137 μm. For the smaller chromite grains all 180–250 μm grains were analysed with a 47 μm beamsize whereas the

Table 1 $^{40}Ar/^{39}Ar$ analytical results from Glen Gollaidh phlogopite separates

	Integrated		Plateau								Inverse isochron						
Aliquot	Integrated age (Ma)	± 2σ (Ma)	Plateau age (Ma)	± 2σ w/J	MSWD	Probability	Steps	N	N-total	%gas	^{39}Ar (mol)	Inverse isochron age (Ma)	±2σ w/J	n	MSWD	p	$^{40}Ar/^{36}Ar(i)$	±2σ
1	361.0	15.0	360.9	4.7	1.90	0.13	E-H	4	7	93.4	1.4×10^{-15}	361.9	3.5	4	1.35	0.26	218	102
2	359.7	8.8	358.4	4.7	2.60	0.07	C-E	3	9	67.8	9.8×10^{-16}	357.1	3.6	3	1.26	0.26	433	151
3	358.9	5.3	359.6	10.0	4.10	0.02	B-D	3	10	85.0	1.6×10^{-15}	358.3	3.6	3	3.45	0.06	426	211
4	361.0	10.0	361.5	4.7	2.10	0.05	B-H	7	9	97.5	1.1×10^{-15}	360.7	3.6	7	2.08	0.06	375	143
4	361.0	10.0	361.5	4.7	2.10	0.05	B-H	7	9	97.5	1.1×10^{-15}	360.7	3.6	7	2.08	0.06	375	143
5	364.0	11.0	360.7	7.6	2.90	0.03	B-E	4	11	86.0	8.9×10^{-16}	360.4	9.3	4	4.30	0.01	316	415
Composite			360.3	4.9	3.50	0.00	B-H	21	21	100.0	5.9×10^{-15}	359.6	3.3	21	3.34	0.00	358	82

J = neutron flux. 2σ uncertainties take account of uncertainties on flux monitors, which is standard practice
MSWD = mean square of weighted deviates
n = number of heating steps in the plateau
p = probability that residuals can be explained by measurement errors alone
(i) = initial Ar

larger (>250 μm) grains were measured with a 105 μm beam size (except for repeat analyses on grains G13–6_86 and G13–6_94 at 47 μm). Silicon (measured on mass 29) was used as an internal standard for olivine analyses, Ca (mass 43) for clinopyroxene and Al (mass 27) for chromite, based on EPMA analyses. Standardisation was achieved against NIST612 glass (Hollocher and Ruiz 1995) and with further quality assurance against garnet (Mongolian garnet MU53388; Norman et al. 1996) for clinopyroxene analyses and metallic CAN-MET (unpublished data from Jung-Woo Park, Canberra; written communication) and Ellendale chromite (P2; unpublished data from Wayne R Taylor, Perth; written communication) standards for chromite. Due to $^{53}Cr^{40}Ar$ interference during analyses of chromites, measurement of ^{93}Nb, and hence Nb concentrations, are subject to an unquantified inaccuracy of up to ~33% over the variance in instrument precision (2σ in Table 2). This value derives from the difference between the average ratio of Nb to Ta in modelled mantle reservoirs (18; Sun and McDonough 1989) and the measured ratios of Nb to Ta (median of 24). It is unclear whether further fractionation between Nb and Ta has a negative influence on this ratio. However, the uncertainty is likely an over-estimate as Dare et al. (2014) report a gas flow dependent $^{53}Cr^{40}Ar$ interference of 9.6%. In any case, Nb values should be considered as maximums thus Ga/Nb ratios are minimums.

Processed data for representative grains are presented in Table 2 with analyses of the NIST612 standards (Supplementary Table 2) and natural reference minerals (Supplementary Table 3) lodged in the supplementary data appendix. Analyses of standard materials showed good reproducibility and similarity to independently-derived data. Sinusoidal grain G13–6_75 is a small grain showing a porous or included texture on polishing, otherwise all grains featured in Table 2 presented a homogeneous texture and even polish.

Results

Age determination

Sample characterisation is key to interpretation of phlogopite Ar/Ar data (Phillips 2012) and to that end the identification of analysed phlogopites as largely phenocrystic grains warrants caution in their age interpretation. Five reproducible step-heatings of phlogopite multi-grain aliquots yield a late Devonian composite plateau age of 360.3 ± 4.9 (2σ) Ma (Fig. 3; Table 1). Due to the excessive scatter in the data, within and between aliquots, MSWD is high (3.5) and p is low. To account for this scatter, the uncertainty is expanded by the square root of MSWD and by Student's t, providing a more realistic measure of the age uncertainty. The relatively flat release spectra and level of reproducibility between aliquots suggest that the age records a simple rapid cooling event consistent with volcanic emplacement. The phlogopite argon data show no evidence for significant excess argon in the inverse isochron correlation diagrams. This is inconclusive however, since the points on the correlation diagrams are nearly all 100% radiogenic, i.e., little dispersal on the isochron and therefore the trapped component composition tends to be poorly defined. As phlogopite is notorious for containing excess argon (Phillips and Onstott 1988; Kelley and Wartho 2000), especially in phenocrysts and xenocrysts, a conservative interpretation would be that the 360 Ma age for these samples represents a maximum age constraint. Two of the release spectra (aliquots 2 and 5) show hints of a 'saddle' shape, potentially indicative of excess argon. Removal of these two aliquots from the composite yields an age of 360.7 ± 3.7 (2σ) Ma, indistguishable from the accepted age above, suggesting that if excess argon is present in some of the grains, it's effects are subtle and do not resolvably impact the age estimate. This leads us to suggest that the 360.3 Ma age reflects an emplacement age rather than a maximum age. The flatness of the age spectra also argue against reheating events at or below the closure temperature. If the deposit was reheated (post emplacement) at temperatures above the closure temperature, ca. 400–480 °C, for a sufficient time, then the argon system could have been partially to completely reset. However, such an event would be recognizable in the petrology of the sample and it's setting, e.g., low to mid-grade metamorphic facies host rocks, for which there is no evidence.

Mantle mineral recovery

Inspection of heavy mineral concentrates recovered abundant chromites, Cr-diopsides (in both size fractions) and four olivine grains (>0.25 mm). No perovskite, picro-ilmenite or garnet was identified by this method (although a few 1–3 mm rounded brownish-red grains of what may be altered garnet occur on the weathered surface of one hand sample). The paucity of recovered olivine is interpreted to be due to serpentinisation, and recrystallisation of xenocrysts to fine grain sizes which disaggregate on sample preparation. While all fifteen quality-control tracer diamonds were recovered during caustic fusion treatment, the aillikite was found to be barren of diamond to the minimum size of 75 μm tested.

Mineral chemistry

Olivine

Olivines are Mg-rich (Fo_{91} – Fo_{89}) with three of four grains over Fo_{90}, typical of mantle-derived olivine. Ni contents are also high, in excess of 3000 ppm (Table 2), consistent with aillikites, and in particular Type Ia kimberlites from the NAC in West Greenland (Garnet Lake; Hutchison and Frei 2009).

Table 2 Representative chemical compositions of clinopyroxene (a), spinel (b) and olivine (c) macrocrysts from the Glen Gollaidh aillikite

(a) Data for clinopyroxenes														
Grain	G13–6 75		G13–6 39		G13–6 47		G13–6 08		G13–6 55		G13–6 41		G13–6 73	
Class	CGP		CLS		CLS		CLS		CLS		CLS		CGP	
Trend	Sinuous		Flat		Flat		LREE-rich		LREE-rich		HREE-rich		HREE-rich	
EPMA results (wt%)														
Oxide	*n* = 6	±2 σ	n = 6	±2 σ	n = 6	±2 σ	*n* = 3	±2 σ	n = 6	±2 σ	n = 6	±2 σ	n = 6	±2 σ
SiO_2	53.83	0.92	52.16	0.25	52.98	0.67	53.12	0.08	53.00	0.70	52.28	0.63	52.47	0.31
TiO_2	0.03	0.01	0.44	0.02	0.29	0.01	0.24	0.002	0.30	0.01	0.36	0.01	0.12	0.01
Al_2O_3	2.68	2.10	6.31	0.10	5.34	0.15	4.00	0.06	4.80	0.07	6.36	0.11	3.66	0.32
Cr_2O_3	1.55	0.29	0.78	0.02	1.44	0.02	1.01	0.01	1.15	0.03	0.75	0.01	0.94	0.07
FeO[a]	1.83	0.22	2.72	0.10	2.34	0.05	2.58	0.06	2.60	0.11	2.52	0.09	2.21	0.23
MnO	0.07	0.02	0.09	0.01	0.08	0.01	0.10	0.01	0.09	0.01	0.08	0.02	0.07	0.01
NiO	0.04	0.01	0.04	0.01	0.04	0.01	0.05	0.01	0.05	0.02	0.04	0.01	0.04	0.01
MgO	16.39	0.73	15.20	0.13	15.81	0.12	16.59	0.13	16.28	0.28	15.29	0.12	16.67	0.50
Na_2O	1.10	1.09	1.59	0.07	1.87	0.10	1.16	0.03	1.42	0.04	1.61	0.06	0.42	0.03
CaO	23.19	2.41	21.10	0.24	20.24	0.08	21.44	0.07	20.99	0.18	21.19	0.19	23.52	0.69
Total	99.94		100.02		99.70		100.28		100.10		100.10		99.65	
La-ICP-MS results (ppm)														
Element[b]	*n* = 1	±2 σ	n = 1	±2 σ	n = 1	±2 σ	*n* = 2	±2 σ	n = 1	±2 σ	n = 1	±2 σ	n = 1	±2 σ
P (31)	84	22	49.6	1.7	32.21	0.93	44.95	1.7	23	0.73	23.21	0.98	16.86	0.67
Sc (45)	128	2	66.42	0.53	74.56	0.54	61.98	0.77	42.01	0.39	63.34	0.43	71.7	0.81
Ti (49)	303	10	2833	20	1874	13	1591.5	17	1889	12	2371	15	695.4	5.8
V (51)	310.7	2.2	274.9	2.3	288.4	2.9	227.6	2.2	289.3	2.9	274.4	2.2	243.2	2.3
Cr (53)	9573	93	5184	48	9841	95	6727	69	7983	80	4907	42	5730	59
Mn (55)	615	4.5	712.7	5.4	642.4	5.5	680.95	6.6	680.9	6.9	681.9	6.6	598.3	6.7
Co (59)	17.21	0.22	19.92	0.2	21.52	0.22	21.96	0.28	23.12	0.28	20.15	0.24	20.81	0.29
Ni (60)	314	2.8	324.2	2.6	373.4	4.3	368.45	4.6	390.9	3.2	336.3	3.1	355.4	3.4
Ga (69)	3.4	0.15	3.74	0.06	3.29	0.07	3.94	0.11	3.99	0.07	3.63	0.079	1.87	0.06
Rb (85)	3.16	0.08	bld	–	bld	–	bld	–	0.15	0.01	0.37	0.019	0.2	0.02
Sr (88)	297	15	128.7	1.1	113.61	0.52	186.5	1.5	54.6	0.36	8.57	0.25	50	16
Y (89)	2.81	0.11	16.34	0.2	8.79	0.08	5.40	0.1	2.71	0.03	15.46	0.14	5.85	0.06
Zr (91)	5.73	0.49	9.14	0.16	40.18	0.52	74.54	1	18.42	0.25	3.60	0.092	3.18	0.11
Nb (93)	4.54	0.23	0.68	0.04	0.22	0.01	0.38	0.01	0.47	0.01	0.109	0.007	0.12	0.02
Ba (137)	123[c]	11	3.86	0.34	0.082	0.02	0.07	0.02	3.93	0.14	8.5	1.3	18.1	4.3
La (139)	10.46	0.23	7.90	0.06	1.92	0.02	4.31	0.05	1.93	0.02	0.070	0.004	0.62	0.19

Table 2 (continued)

Ce (140)	22.21	0.32	18.35	0.25	6.55	0.05	17.65	0.17	5.88	0.05	0.167	0.007	1	0.23
Pr (141)	2.49	0.04	1.94	0.02	1.10	0.01	3.01	0.04	0.88	0.01	0.086	0.003	0.12	0.02
Nd (146)	9.04	0.2	7.02	0.06	5.99	0.07	14.49	0.18	4.18	0.06	1.04	0.02	0.52	0.07
Sm (147)	1.33	0.054	1.65	0.03	1.75	0.03	3.11	0.07	1.06	0.02	0.88	0.02	0.153	0.009
Eu (153)	0.42	0.01	0.65	0.01	0.62	0.012	0.87	0.02	0.34	0.01	0.42	0.01	0.067	0.003
Gd (157)	0.81	0.05	2.15	0.04	1.80	0.037	2.14	0.06	0.98	0.03	1.72	0.03	0.35	0.01
Tb (159)	0.09	0.01	0.41	0.01	0.28	0.004	0.27	0.01	0.127	0.004	0.351	0.006	0.089	0.004
Dy (163)	0.49	0.03	2.83	0.04	1.72	0.03	1.34	0.04	0.68	0.02	2.64	0.04	0.85	0.02
Ho (165)	0.10	0.006	0.64	0.01	0.35	0.01	0.22	0.01	0.112	0.004	0.604	0.009	0.220	0.005
Er (166)	0.34	0.02	1.93	0.02	1.00	0.02	0.55	0.02	0.24	0.01	1.83	0.03	0.74	0.01
Tm (169)	0.06	0.003	0.27	0.01	0.13	0.003	0.068	0.003	bld	–	0.258	0.004	0.115	0.003
Yb (172)	0.50	0.018	1.87	0.03	0.89	0.02	0.42	0.02	0.15	0.01	1.78	0.02	0.83	0.02
Lu (175)	0.09	0.003	0.26	0.01	0.12	0.003	0.057	0.003	0.016	0.001	0.249	0.005	0.120	0.004
Hf (178)	0.09	0.01	0.54	0.02	1.26	0.03	1.66	0.06	0.74	0.03	0.36	0.02	0.12	0.01
Ta (181)	0.09	0.008	0.05	0.004	0.03	0.002	0.062	0.006	0.033	0.003	bld	–	bld	–
Pb (208)	0.51	0.09	0.78	0.03	0.26	0.01	0.31	0.02	0.18	0.01	bld	–	0.07	0.01
Th (232)	0.86	0.02	1.48	0.03	0.16	0.01	0.18	0.01	0.069	0.004	bld	–	bld	–
U (238)	0.39	0.03	0.39	0.01	0.03	0.003	0.055	0.005	0.019	0.002	0.014	0.002	bld	–
(b) Data for spinels														
Grain	G13–6 86		G13–6102		G13–6124		G13–6146		G13–6142		G13–6142		G13–6 94	
Class	MC		MAC		MAC		MAC		MAC		TMAC[d]		TFMAC	
EPMA results (wt%)														
Oxide	n = 3	±2 σ	n = 3	±2 σ	n = 3	±2 σ	n = 3	±2 σ	n = 3	±2 σ	n = 3	±2 σ	*n* = 5	±2 σ
SiO_2	0.05	0.01	0.07	0.00	0.06	0.01	0.08	0.02	0.09	0.02	0.13	0.02	0.29	0.36
TiO_2	0.08	0.02	0.37	0.01	0.30	0.00	0.27	0.00	0.11	0.00	1.13	0.76	5.00	1.13
Al_2O_3	19.91	0.15	40.89	0.12	35.98	0.06	25.94	0.27	30.37	0.04	22.14	2.69	15.00	2.60
Cr_2O_3	47.21	0.12	25.69	0.15	27.84	0.07	41.37	0.13	39.28	0.05	41.55	5.61	29.79	5.64
FeO[a]	16.86	0.27	12.22	0.19	18.11	0.26	18.08	0.30	14.28	0.09	19.84	6.71	34.73	4.87
MnO	0.22	0.02	0.14	0.00	0.20	0.03	0.24	0.03	0.19	0.02	0.21	0.05	0.32	0.04
NiO	0.13	0.02	0.26	0.03	0.22	0.00	0.16	0.01	0.18	0.00	0.19	0.02	0.19	0.02
MgO	13.89	0.06	18.38	0.11	15.73	0.06	14.68	0.10	16.50	0.16	15.56	0.90	13.44	0.61
CaO	0.00	0.00	0.00	0.00	0.00	0.00	0.00	0.00	0.00	0.00	0.03	0.01	0.10	0.05
Total[e]	98.44	0.47	98.14	0.34	98.55	0.25	100.95	0.52	101.12	0.27	100.89	1.65	98.94	2.05
La-ICP-MS results (ppm)														
Element[b]	n = 2	±2 σ	n = 1	±2 σ	n = 1	±2 σ	n = 1	±2 σ	n = 1	±2 σ	n = 1	±2 σ	n = 2	±2 σ
Sc (45)	3.64	0.1	1.02	0.07	2.55	0.14	4.1	0.26	1.48	0.18	4.55	0.2	11.28	0.41
V (51)	1164.5	13	655.3	5	867.4	6.6	1167	14	643.5	7.3	824	17	569.5	13.15
Co (59)	273.7	4.3	217.5	3.1	252.8	3.1	270.6	4.7	189.6	2.2	249.1	5.2	206	4
Cu (65)	8.655	0.36	4.18	0.24	5.32	0.26	7.45	0.67	6.29	0.54	9.48	0.87	4.4	0.5
Zn (66)	1090	38	836	17	977	21	1204	37	817	18	1156	29	1510	37
Ga (69)	22.35	0.59	57.12	0.99	57.47	0.97	41.8	1.2	25.62	0.66	55.7	2.1	90	2
Ge (72)	1.63	0.13	1.46	0.10	1.76	0.13	1.58	0.33	1.0	0.2	3.0	0.4	4.05	0.32
Sr (88)	0.07	0.02	bld	–	bld	–	bld	–	bld	–	100	5	85	7
Y (89)	bld	–	bld	–	bld	–	bld	–	bld	–	1.31	0.11	2.27	0.22
Zr (90)	0.549	0.049	0.19	0.03	0.09	0.02	0.25	0.06	0.15	0.04	20.9	1.1	27.79	1.09

Table 2 (continued)

Nb (93)[f]	0.369	0.02	0.10	0.02	0.16	0.02	0.28	0.05	0.13	0.03	9.09[g]	0.99	9.38[g]	0.58
Sn (118)	0.6445	0.052	0.56	0.07	0.60	0.08	0.47	0.18	0.46	0.16	1.62	0.27	3.64	0.26
Ba (137)	0.25	0.11	bld	–	bld	–	bld	–	bld	–	282[g]	38	184[g]	14
Hf (178)	bld	–	bld	–	bld	–	bld	–	bld	–	0.43	0.07	0.88	0.08
Ta (181)	0.016	0.004	bld	–	bld	–	bld	–	bld	–	0.57	0.06	0.43	0.03
(c) Data for olivines														
Grain	G13–6 01		G13–6 02		G13–6 03		G13–6 04							
EPMA results (wt%)														
Oxide	n = 3	±2 σ	n = 3	±2 σ	n = 3	±2 σ	n = 3	±2 σ						
SiO_2	40.40	0.72	39.93	0.38	40.31	0.23	40.56	0.10						
TiO_2	0.01	0.01	0.01	0.00	0.01	0.00	0.01	0.01						
Al_2O_3	0.01	0.01	0.01	0.00	0.02	0.00	0.02	0.00						
FeO[a]	9.26	0.20	10.48	0.31	9.73	0.19	9.63	0.33						
MgO	50.32	0.00	49.23	0.00	49.72	0.01	49.58	0.00						
Na_2O	0.01	0.06	0.01	0.11	0.01	0.30	0.01	0.12						
Total[h]	100.63	0.87	100.30	0.28	100.42	0.44	100.42	0.46						
La-ICP-MS results (ppm)														
Element[b]	n = 2	±2 σ	n = 1	±2 σ	n = 1	±2 σ	n = 1	±2 σ						
P (31)	97.3	1.6	102.6	2.7	40	1.4	40.6	1.3						
Ti (49)	23.09	0.82	39.3	1.5	46.2	1.4	45.1	1.1						
V (51)	2.59	0.08	3.22	0.09	4.07	0.10	4.02	0.10						
Cr (53)	62.8	1.3	51.7	1.1	109.8	1.6	112	2						
Mn (55)	983	11	942	14	907	11	908	12						
Co (59)	143.4	1.5	156.2	2.2	149.7	1.9	150.6	2						
Ni (60)	3021	29	3057	40	3004	34	3029	42						
Ga (69)[i]	bld	–	0.06	0.01	0.08	0.01	0.09	0.01						
Y (89)	bld	–	bld	–	bld	–	0.067	0.001						
Zr (91)	0.02	0.01	0.02	0.01	0.03	0.01	0.02	0.01						
Yb (172)	0.011	0.003	bld	–	bld	–	bld	–						

Class = mineral classification following Ramsay and Tompkins (1994): CGP = garnet peridotite-associated composition; CLS = spinel lherzolite-associated composition

Trend = shape of chondrite-normalised REE trend

bld = below limit of detection (Yaxley and Kamenetsky 1999)

[a] FeO is total iron

[b] Figures superseding element symbols describe the isotopes on which measurements were performed

[c] Concentration of highly incompatible Ba may be slightly elevated due to melt infiltration. However, concentrations of other incompatible elements are consistent with published data from other Scottish localities (Hughes et al. 2015) so while unquantifiable, the deviation from primary clinopyroxene Ba concentration is not considered high

[d] Analyses performed on the rim of the grain

[e] EPMA analysis total accounts for ZnO, elemental concentration is quoted as determined by laser ICP-MS due to higher precision

[f] 2σ uncertainty are within-run errors based on measurement analytical variance however, due to Cr^{53} Ar^{40} interference on ^{93}Nb, Nb concentrations are subject to a further unquantified uncertainty of up to ~30%

[g] Concentration of highly incompatible Ba and Nb may be elevated due to melt infiltration

[h] EPMA analysis total accounts for P_2O_5, NiO, Cr_2O_3 and MnO; elemental concentrations are quoted as determined by laser ICP-MS due to higher precision

[i69] Ga can be affected by interference with $^{53}Mn^{16}O$ but Mn concentrations are too low to have an effect in addition to analytical uncertainty

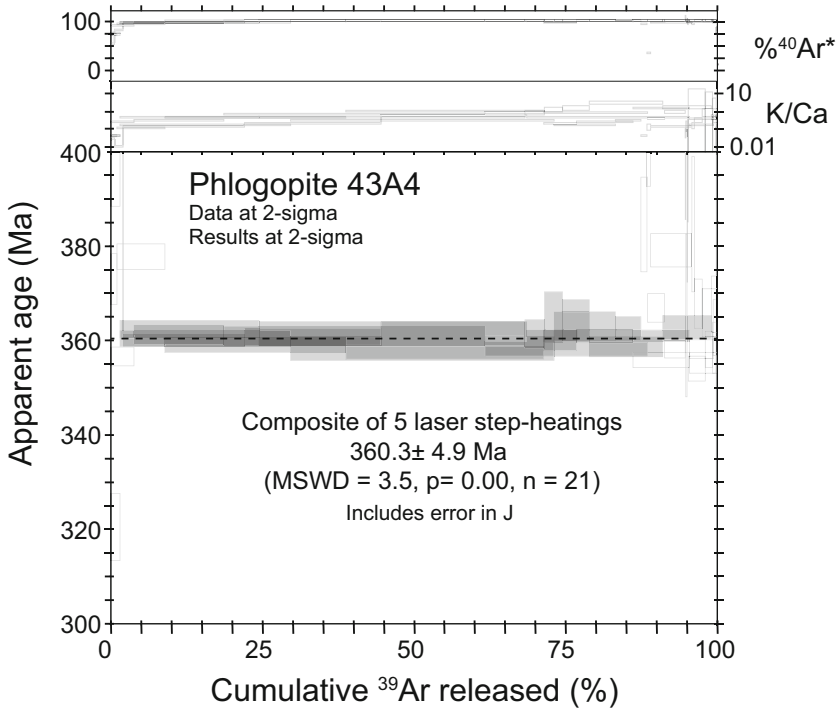

Fig. 3 $^{40}Ar/^{39}Ar$ apparent composite age spectra for Glen Gollaidh phlogopite separates showing percentage of radiogenic ^{40}Ar, K/Ca ratio and cumulative ^{39}Ar fraction versus age. Uncertainty in J is excluded for plateau definition, but included for final age calculation. Age represents a composite of steps from five independently determined plateaus. These steps are combined and inverse variance weighted to generate an average age

Clinopyroxene

Clinopyroxene compositions range from 2.6–6.6 wt% Al_2O_3 and 19.9–23.9 wt% CaO encompassing, at one place, most of the 'remarkable range' (Upton et al. 2011) exhibited by Scottish mantle-derived clinopyroxenes compared to world-wide xenolith localities. Based on Cr and Al content (Ramsay and Tompkins 1994), the majority of Cr-diopsides are consistent with spinel lherzolite compositions (CLS) although a significant proportion (30% of grains) also plots in the garnet peridotite (CGP) field with Cr_2O_3 content up to 1.56 wt% (Fig. 4). Glen Gollaidh clinopyroxenes do not exhibit the

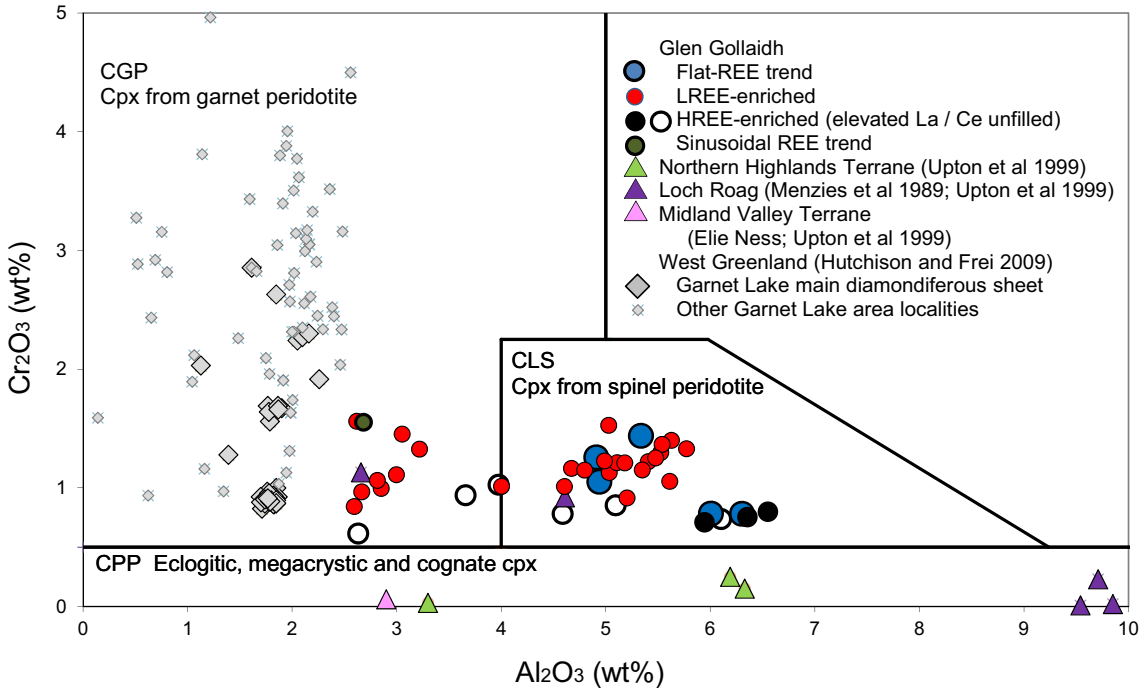

Fig. 4 Compositions of Glen Gollaidh clinopyroxene xenocrysts discriminated on the basis of Cr_2O_3 and Al_2O_3 content. Classification follows the methodology of Ramsay and Tompkins (1994). Rare-earth element (REE) trends refer to characteristics shown in Fig. 5

Al_2O_3 depletion (<2.5 wt%) evident in samples derived from well within the diamond stability field (Hutchison and Frei 2009). However, the compositional range is similar to Loch Roag (Menzies et al. 1989; Upton et al. 1999). Loch Roag, further localities in the Northern Highlands Terrane (Upton et al. 1999) and Elie Ness in the Midland Valley Terrane (Upton et al. 1999) all include eclogitic / megacrystic / cognate clinopyroxenes which are not represented at Glen Gollaidh.

Cr-diopsides express four distinct rare-earth element (REE) trends. 1) Of 41 grains, the most common trend (63% of grains) shows a light rare-earth elements (LREE) enrichment up to 50 times chondritic concentrations, to chondritic values amongst the heavy rare-earth elements (HREE) (Fig. 5). This trend mirrors the composition of CGP from the Garnet Lake aillikite (Hutchison and Frei 2009) albeit with slightly smaller Nd/Yb ratios (Fig. 5). The LREE-enriched trend also mirrors – although with lower absolute REE concentrations – eclogitic, megacrystic or cognate (CPP) clinopyroxene from further north in the Northern Highland Terrane at Rinibar (Bonadiman et al. 2008; Upton et al. 2011), further south at Gribun, and at Loch Roag, Isle of Lewis (Hebridean Terrance; Upton et al. 1999). 2) A further 22% of Glen Gollaidh clinopyroxene grains show the opposite trend: Nd and Sm have chondriditic values and HREE are up to 10 times chondrite concentrations. Spinel-peridotite affinities in major element compositions are twice as abundant as

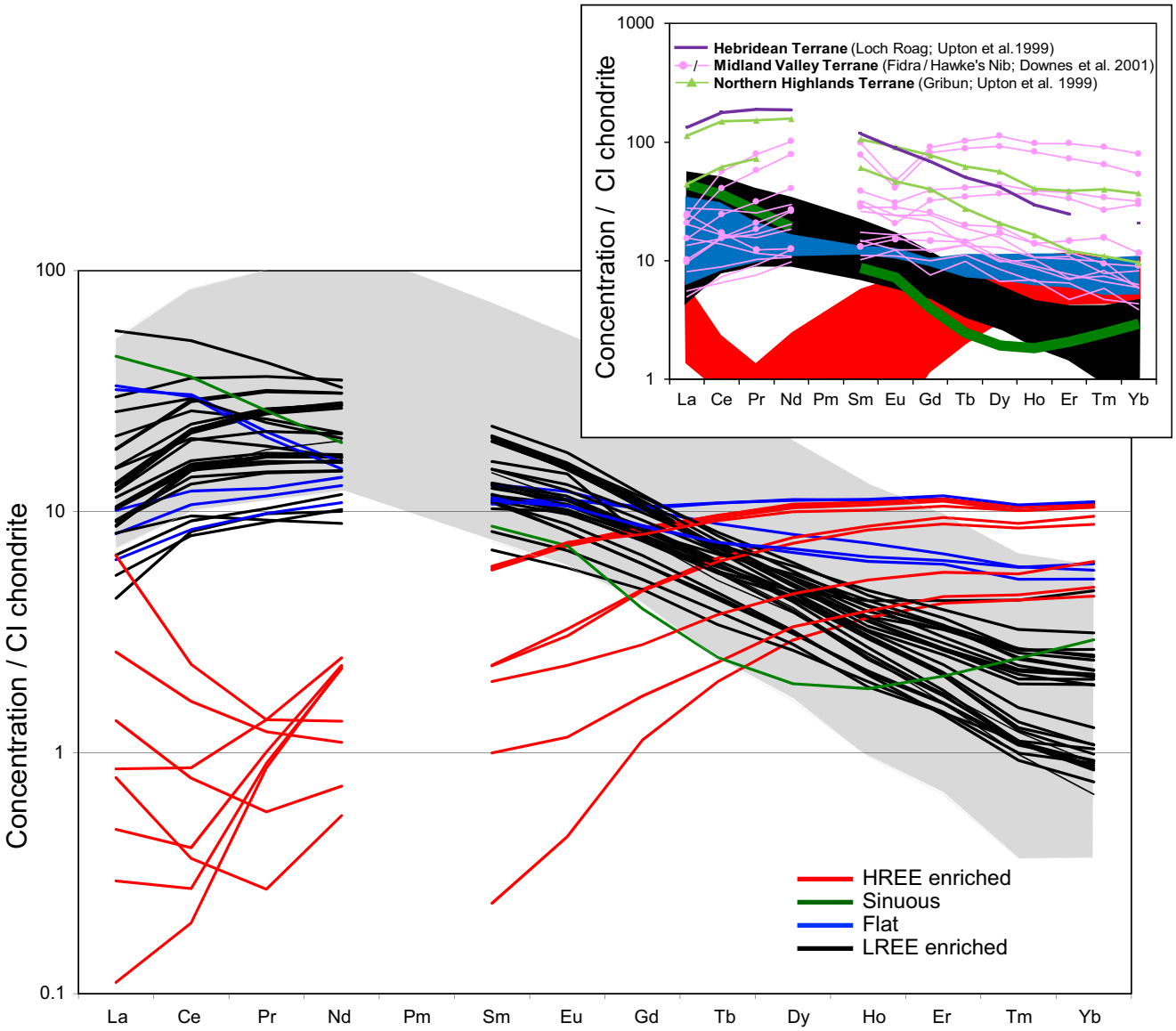

Fig. 5 Rare-earth element (REE) compositions of Glen Gollaidh clinopyroxene xenocryst concentrates normalised to CI chondrite (McDonough and Sun 1995). main figure The range of clinopyroxene compositions from the Garnet Lake aillikite, representative of the NAC in West Greenland (3 samples – Hutchison and Frei 2009 – and further unpublished data) is represented by the grey field. Inset The Glen Gollaidh analyses are expressed as trends with data from other Scottish clinopyroxenes grains superimposed

garnet-peridotite compositions in both HREE- and LREE-enriched clinopyroxenes. However, the HREE-enriched clinopyroxenes are lower in Cr_2O_3 content than the LREE-enriched grains (Fig. 4). The HREE-enriched trend can be further subdivided based on elevated or depleted chondrite-normalised La and Ce compared to Pr. It is notable (Fig. 4; filled black symbols) that the La and Ce depleted samples lie furthest into the spinel peridotite field. No similar clinopyroxene HREE-enriched distributions like those at Glen Gollaidh are seen in other Scottish mantle sample-bearing rocks. 3) Five grains (12% of all grains; all with CLS compositions) show a flat REE trend (Fig. 5) consistently close to 10 times chondritic concentrations matching trends from the Midland Valley Terrane at Fidra, and in particular at Hawke's Nib (Downes et al. 2007) and at Streap Com'laidh in the Northern Highland Terrane (Upton et al. 2011). 4) A single CGP outlier (G13–6 75) shows a sinuous trend – LREE enriched and with a minimum at Dy (0.49 ppm) – resembling the average clinopyroxenes from Rinibar (Hughes et al. 2015).

Cryptic melt infiltration into mantle minerals has been reported from kimberlites (Aulbach and Viljoen 2015) and can have an influence on trace element chemistry by raising concentrations, particularly for incompatible elements. Similar infiltration into mantle minerals may in theory have occurred in Glen Gollaidh aillikites. High values for elements such as Ba, Nb and Rb in some analyses could be influenced by the presence of microscopic melt inclusions and the unusual sinuous characteristic of the single CGP grain outlier draws particular attention. However, Glen Gollaidh clinopyroxenes exhibit similar or lower REE concentrations compared to grains from other Scottish localities (Fig. 5). Furthermore, for all analyses (with the exception of the sinuous REE- pattern grain G13–6 75) Ba, Rb and Nb concentrations are consistent with published values from other localities, particularly for clinopyroxenes from Fidra (Upton et al. 1999) and Loch Roag (Hughes et al. 2015). In order to assess the effect of infiltration, Aulbach and Viljoen (2015) compare melt / clinopyroxene partition coefficients with compositions of bulk kimberlite and clinopyroxene grains. In the case of Glen Gollaidh, the large clinopyroxene grains are xenocrysts and thus aillikite / clinopyroxene partition coefficients are of little relevance. However, bulk compositional data provide knowledge of the composition of possible infiltrating fluid and are thus provided in Supplementary Table 1. Bulk rock compositions of ten Glen Gollaidh aillikite samples from three localities provide consistent REE compositions evenly declining from La at 500-times to Yb at 10-times CI chondrite concentrations. REE concentrations coincide with the more light REE-enriched samples from the Tugtutôq-Nûgârmiut mela-aillikites at the Greenlandic margin of the NAC in the Gardar province (Upton et al. 2006). No combination of any Glen Gollaidh bulk chemical data with any other clinopyroxene type can reproduce the highly depleted mid-heavy REE trend seen in the sinuous clinopyroxene grain G13–6 75. While rare at Glen Gollaidh, given that similar compositions are common at Rinibar (including for incompatible elements Nb and Rb; Hughes et al. 2015) its composition is concluded to be genuine.

Orthopyroxene has been identified optically in lherzolite xenoliths but compositions have not been determined. In the absence of orthopyroxene recovery from mineral separates, calculations using the opx-cpx solvus thermometer (Bertrand and Mercier 1985) have been made assuming that equilibrium orthopyroxene is end-member $MgSiO_3$ enstatite – providing *minimum* temperature estimates. Results show (Fig. 6) that Cr-diopside compositions require at least 19 kbar (59 km) to give an average minimum temperature of 961 °C. Given the spread of data, this is the lowest pressure at which the temperature was cool enough for some clinopyroxene compositions to coincide with a 40 mWm^{-2} geotherm (Hasterok and Chapman 2011). Grütter (2009) cites 40mWm^{-2} as a globally typical cratonic mantle geotherm. However, geotherms in the

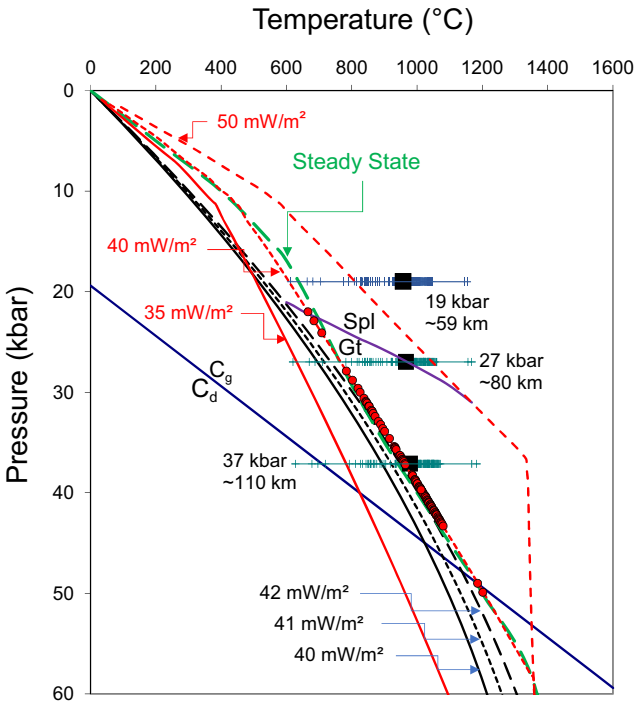

Fig. 6 Modelled Glen Gollaidh clinopyroxene minimum equilibrium temperatures in the context of mantle geotherms (40, 41 and 42 mWm^{-2} in black, Chapman and Pollack 1977; Steady State, in green, McKenzie et al. 2005; 35, 40 and 50 mWm^{-2}, in red, Hasterok and Chapman 2011), the spinel (Spl) to garnet (Gt) transition in peridotites (Grütter 2009) and diamond (C_d) / graphite (C_g) stability (Kennedy and Kennedy 1976). Temperature calculations are modelled on 19, 27 and 37 kbar following the methodology of Bertrand and Mercier (1985). Isobaric temperatures calculated for individual grains are represented by crosses, averages for each pressure increment are shown by solid squares. As equilibrium with end-member enstatite is assumed, all temperature estimates are minimums. Depth calculations are based on Dziewonski and Anderson (1981). Temperatures along the preferred 40 mWm^{-2} geotherm of Hasterok and Chapman (2011) are shown with red circles

vicinity of the NAC are reported as 36 mWm^{-2} in West Greenland (Sarfartoq at 529 Ma; Grütter and Tuer 2009) and 38 mWm^{-2} in Quebec, Canada (Renard at 630 Ma; Grütter et al. 2006). Identification of unaltered orthopyroxene in equilibrium with clinopyroxene in mantle xenoliths would allow more robust geothermometry. However, it can be confidently stated that 19 kbar is the minimum equilibrium pressure for any measured Glen Gollaidh Cr-diopside. An average Cr-diopside (with composition equivalent to a temperature of 979 °C) requires a pressure of 37 kbar (Fig. 6), equivalent to conditions at 110 km in depth (Dziewonski and Anderson 1981), to lie even on a locally warm (40 mWm^{-2}) geotherm. Thus geothermometry places typical mantle components from the dyke close to the spinel-garnet transition (although average Cr-diopsides likely derive from firmly within the graphite stability field). This observation is consistent with independent conclusions based on clinopyroxene (and chromite) chemistry. Furthermore, and assuming a mantle geotherm of 40 mWm^{-2}, an iterative approach to calculating pressures and temperatures using the Bertrand and Mercier (1985) opx-cpx solvus thermometer also shows the Glen Gollaidh clinopyroxenes to have derived from a range of depths crossing the spinel to garnet lherzolite transition and with some rare grains extending into the diamond stability field (Fig. 6).

Chromite

All analysed spinels are chromites. Of 45 grains analysed for major element chemistry, a single Mg chromite (which dominate the population at Clare Island, Eire; Upton et al. 2001), two Ti–Fe–Mg–Al chromites and one Ti–Mg–Al chromite were identified (following the classification scheme described in Hutchison 2011). The remaining, and large majority of grains, are Mg–Al chromites. Ubiquitous Mg–Al chromite is otherwise seen further west at Loch Roag and north-east at Rinibar (Upton et al. 2011). In contrast, further south in Scotland, alkaline igneous rock-hosted spinel xenocrysts are dominated by Al spinel (Upton et al. 2011).

One Mg–Al chromite was identified with a Ti–Mg–Al chromite composition rim and another has a Ti–Fe–Mg–Al chromite rim. This is the same trend described in the NAC at Garnet Lake (Hutchison and Frei 2009) and is consistent with cognate groundmass chromite crystallisation on xenocrystal seed grains. All Glen Gollaidh chromite compositions coincide with chromites in kimberlites and within the garnet peridotite field (based on Ti and Cr content; Grütter and Apter 1998). All chromites also describe the spinel Magmatic Trend 2 (Mitchell 1986) based on divalent / trivalent cations. Compositions are therefore consistent with chromites from world-wide kimberlites and lamproites and in particular spinel xenocrysts from the Garnet Lake aillikite (Hutchison and Frei 2009). In no cases are the Cr contents (<47.2 wt% Cr_2O_3) abundant enough to be consistent with the diamond stability field (following the method of Grütter and Apter 1998). Major element chemistry therefore shows the Glen Gollaidh chromites to be consistent with mantle xenoliths and similar to aillikites and kimberlite with a shared geological history elsewhere on the NAC.

Trace elements are particularly useful in assessment of the petrological affinities of xenocrystal chromites (in addition to those from unknown sources such as are encountered in mineral exploration). Nb stands out as being the most valuable element for this purpose. The large uncertainty (~33%) in Nb compositions may appear to pose a significant problem in the utility of this element. However, discrimination diagrams use $\log_{10}$ ratios and hence are resistant to uncertainties of this magnitude. Figure 7 shows Glen Gollaidh chromites plotted in terms of $\log_{10}$(Ga/Nb) against $\log_{10}$(Co/V). Data are compared to the mantle field of Yaxley (2008; developed by Taylor WR, Australian National University's Research School of Earth Sciences). Compositions from regional samples from the North Australian Craton (Hutchison 2011) are also included. This data-set has been chosen due to a paucity of NAC chromite trace element data and because the North Australian Craton data express the range of compositions expected from a diamondiferous craton with chromite from a range of crustal and mantle sources (akin to the NAC). Given the high uncertainty of Nb concentrations, as a quality assessment, the same grain analyses have been plotted with Nb replaced with concentrations of Ta × 18. The same distribution of grains between the mantle field and magmatic array were identified. Figure 7 shows that the Mg chromite grain lies clearly within the mantle array compared to the Mg–Al chromites which describe a spread towards shallower magmatic compositions with the range in compositions likely reflecting both a range of depths of origin and the influence of mantle metasomatism (Hughes et al. 2015). The Ti-bearing chromites (whole grains and rims) lie within the mantle array as a consequence of elevated Nb (also exhibiting similarly elevated Ta).

Discussion

The Glen Gollaidh aillikite provides the opportunity to address where the locality lies in the context of the margin of the NAC mantle lithosphere. The aillikite also gives insights into the mineralogy of the NAC – including diamond prospectivity – and hence its prior geological history.

Glen Gollaidh's place at the NAC margin

The Glen Gollaidh outcrop lies amongst the Neoproterozoic sedimentary rocks of the Moine Supergroup, the hanging-wall of the Moine Thrust which is located ~4 km to the west (Fig. 1). However, the Archean and Proterozoic rocks of the

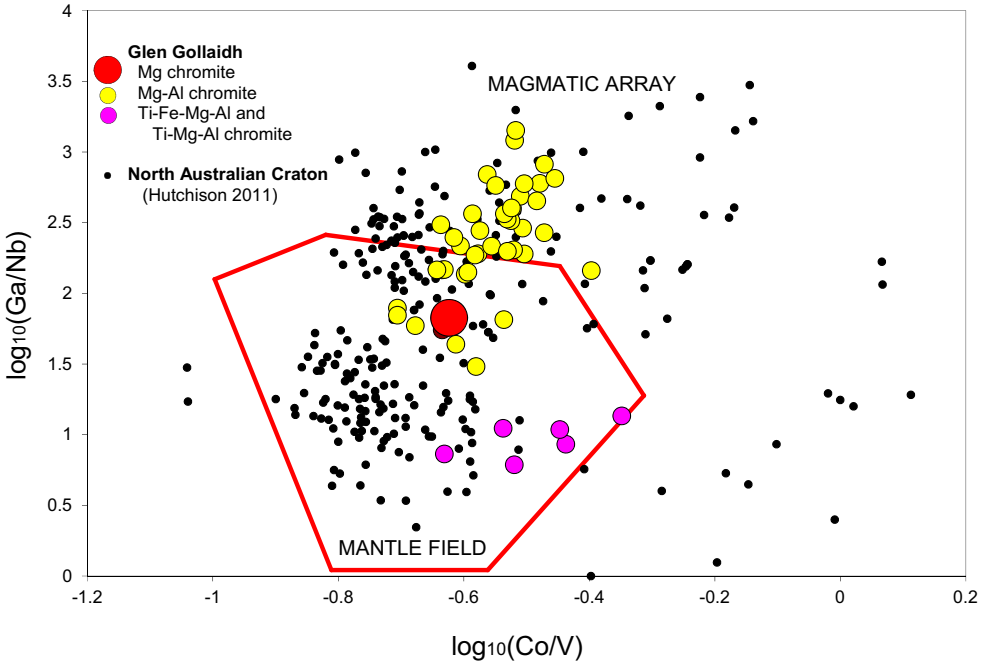

Fig. 7 Compositions of Glen Gollaidh chromite xenocrysts. Mantle field and magmatic array from Yaxley (2008). Glen Gollaidh Ga/Nb values are minimum ratios as Nb data are maximum values. Chromites from regional surface-sediment samples from Northern Territory, Australia are shown to demonstrate the range of compositions expected from a diamond-bearing cratonic region with both kimberlite-hosted and crustal-derived (basaltic) chromites

Lewisian component of the NAC are exposed to the west of the Moine Thrust. The Lewisian rocks comprise part of the reworked NAC mobile belt, most of which is preserved to the north-west in the previously adjoining Greenlandic component, there termed the Nagssugtoqidian Orogen. Hughes et al. (2015) argued that the NAC lithosphere keel is evidenced by mantle xenoliths at Loch Roag, Isle of Lewis. Evidence for an unusually deep mantle source in the context of other Scottish localities is apparent at Glen Gollaidh, and some criteria draw closer comparisons with NAC mantle sources in Greenland. West Greenland comprises what were more central parts of the NAC (as evidenced by deep-sourced peridotitic xenoliths and diamonds; Hutchison and Frei 2009, Wittig et al. 2010). The northern part of the West Greenland NAC is particularly characterised by depleted mantle at shallow depths where clinopyroxene is rare (Sarfartoq, West Greenland, Bizzarro and Stevenson 2003; Ubekendt Ejland, West Greenland, Bernstein et al. 2006). Depletion is due to considerable melt extraction. However, deeper parts of the northern West Greenland NAC and rocks to the south, previously geographically closer to Glen Gollaidh, have seen less melt extraction and, like at Glen Gollaidh, are clinopyroxene-bearing. The clinopyroxenes from the Garnet Lake aillikite (Sarfartoq, West Greenland NAC) occur with garnet and derive from 195 km depth (1258 °C and 62 kbar assuming a 41 mWm^{-2} geotherm; Hutchison and Frei 2009). Chondrite normalised rare-earth patterns from these samples (Fig. 5) best match the dominant Glen Gollaidh clinopyroxene LREE-enriched trend, the closest other Scottish analogue being at Loch Roag (Upton et al. 1999). Mantle components in the Glen Gollaidh aillikite are not as deep-sourced as at Garnet Lake, hence during the late Devonian the cratonic root underlying this part of Scotland was apparently too thin to lie within the diamond stability field. However, mineral chemistry still places the dyke as hosting some of the deepest mantle components recovered in the UK. Minimum pressure estimates for Glen Gollaidh are 22 kbar but more likely greater depths have been sampled, equivalent to 37 kbar and more, consistent with the range in compositions of clinopyroxenes and the (inconclusive) identification of garnet grains. The proximity of Glen Gollaidh to the Moine Thrust sheet and the considerable mantle lithosphere thickness sampled at Glen Gollaidh suggests that the NAC extends at depth to the east of its Lewisian surface expression. A similar conclusion is made by Hughes et al. (2015) for Rinibar, Orkney (Fig. 1). Hughes et al. (2015) also comment that the underlying keel of NAC is not, however, present ~175 km south of Glen Gollaidh at Streap Com'laidh. Estimates for equilibrium conditions for Streap Com'laidh peridotites are 1100–1200 °C at 14–23 kbar (Praegel 1981). A thinning of the NAC margin south and east is also borne out in the dominance of various mantle mineral classes. Anomalous samples occur as garnets reported in Elie Ness, Fife and in Dunaskin Glen and the Heads of Ayr (Upton et al. 2003) with inferred pressures up to 20 kbar. However, more typically, there is also a progression from dominant, deep-sourced Mg chromite (Clare Island; Upton et al. 2001), to Mg–Al chromite (Loch Roag, Upton et al. 2011; with minor Mg chromite, Glen Gollaidh), to Mg-Al chromite with Mg–Cr–Al spinel (Rinibar) to shallow-sourced Mg–Cr–Al spinel (off-craton at Streap Com'laidh and Fidra).

Mantle lithosphere composition

Isotopic and bulk rock trace element data from the Glen Gollaidh aillikite suggest a protolith from highly enriched lithospheric metasomite aggregates (Faithfull 2012; Hughes 2012). On the Isle of Lewis, the Loch Roag monchiquite dyke (Menzies et al. 1989) has a similar enriched trace-element bulk rock signature. Trace element studies of mantle clinopyroxenes from rocks emplaced north of the Great Glen Fault suggest complex metsomatic histories which cannot be attributed to a single event (Upton et al. 2011). High LREE bulk-rock enrichment (seen for other Scottish localities in clinopyroxene compositions; Fig. 5) supports small degrees of melting of previously metasomatised mantle. More likely at Glen Gollaidh, despite the failure to definitively identify garnets, partial melting in equilibration with garnet is implied. This conclusion is supported by the compositions of both spinel and clinopyroxene and geothermometry calculations. It is apparent from other studies (e.g. Upton et al. 2011; Hughes et al. 2015) that the Scottish mantle has experienced an unusually complex history of fragmentation, amalgamation and sporadic metasomatism (compared to the more simple Greenlandic NAC; Wittig et al. 2010). This conclusion is very much borne out at Glen Gollaidh. Groups of distinct clinopyroxene compositions amongst the unusually broad variation seen at Glen Gollaidh likely derive from different mantle depths. The various groups have similarities with different Scottish mantle xenolith localities. The most common clinopyroxenes west at Loch Roag (Upton et al. 1999) are similar to Glen Gollaidh's LREE-enriched grains, typical samples north-east at Rinibar (Hughes et al. 2015) resemble the Glen Gollaidh sinuous-REE clinopyroxenes, and the flat-REE grains are also abundant south in the Midland Valley Terrane occurrences (Fidra and Hawke's Nib; Downes et al. 2007). It is concluded that Glen Gollaidh lies at a convergence which has seen all of these different mantle events.

Late Devonian magmatism

The late Devonian was a quiet period in Scottish geological history. The Iapetus Ocean had been slowly closing since the Cambrian Period with subduction at its margins driving the Caledonian Orogeny, prevalent through Laurentia and as evidenced in rocks extending from Scandinavia, the UK and Greenland to maritime North America (Stephenson 2000). The location around Ben Hope was a part of the Laurentian continent – a large and stable cratonic region – since at least the early Proterozoic until north and west Scotland experienced a series of dramatic Caledonian transpressional faults commencing in the early Ordovician. The Iapetus had closed by the mid-Silurian (ca. 425 Ma; Stone et al. 1993) with the suture between the prior supercontinents of Laurentia and Avalonia lying in what is now the Southern Uplands Terrane of southern Scotland. Caledonian metamorphism associated with the Moine Thrust largely ceased around the same time (429 Ma; Goodenough et al. 2011) with the Loch Borralan intrusion (39 km south-west of Glen Gollaidh) dated to 430 ± 4 (2σ) Ma (Van Breeman et al. 1979) and the Loch Loyal syenite complex (18 km east north-east of Glen Gollaidh) dated to 426 ± 9 (2σ) Ma (Halliday et al. 1987). However, the subducting Avalonia slab continued to progress northwards, first reflected in minor magmatism near the Iapetus suture and subsequently within the regions affected by the Caledonian Orogeny. The final magmatic effects along the suture are seen in the 397 Ma intrusives at Fleet and Criffel (Halliday et al. 1980). In mainland Scotland, minor alkali intrusives and fenitised rocks were intruded along the Great Glen Fault at ca. 390 Ma (Macdonald and Fettes 2007). This age still pre-dates the age of the Glen Gollaidh aillikite by ca. 25 Ma. However. the very last intrusions attributed to Caledonian deformation occurred at the extension of the Great Glen Fault in West Shetland ca. 350–370 Ma (Lancaster et al. 2017). At this point the Caledonian Orogeny had firmly entered an extensional phase. The timing of the Shetland magmatism has been noted as an outlier (Stephenson 2000), suggesting that Shetland occupied a separate terrane from what is now mainland Scotland. However, more or less contemporaneous magmatism in Shetland and Glen Gollaidh suggests that these regions were not significantly geographically distinct, a conclusion supported by the contiguous pattern of sedimentation in the Orcadian Basin (Enfield and Coward 1987).

Magmatism was not seen again in Scotland after the intrusion of the Glen Gollaidh aillikite until intra-plate magmatism which was at its most active from 341 to 335 Ma but occurred considerably further south (Upton et al. 2004). This magmatism, which included the Clyde Plateau basalts (Monaghan and Parrish 2006) is interpreted to be a consequence of hot-spot magmatism and continental collision further south between Gondwana and Laurasia (8°W).

The fact that the maximum age of the Glen Gollaidh aillikite is so much younger than other igneous events along the nearby Moine Thrust is perplexing. However, the key lies with the almost coeval magmatism in Shetland along the extension of the Great Glen Fault. Late Caledonian magmatism in Shetland is attributed to localised melting of the lithospheric mantle as a consequence of sinistral displacements between Laurentia and Baltica (Lancaster et al. 2017). However, the principle driver may be delamination of the subducted Avalonia slab (Lancaster et al. 2017) and hence the same explanation could be attributed to the magmatism at Glen Gollaidh. Delamination as a driver to magmatism contrasts to aillikite magmatism in central West Greenland which is interpreted to have been triggered by rifting (Tappe et al. 2009).

While the variability in chemistry of the Glen Gollaidh mantle component has a partial explanation in a range of sampling depths, the majority of the variability is explained by a complex history of metasomatism and partial melting; a consequence of the upheavals associated with the closure of the Iapetus and accumulation of Laurussia (Macdonald and Fettes 2007). It is concluded that this same complex mantle chemistry created suitable conditions to allow melting of the mantle below Glen Gollaidh at this late stage in the deformations of the margins of the NAC. Furthermore, it appears that at the end of the Devonian, a global change in the physical properties of continental lithosphere was beginning to occur. In the UK and Eire, basaltic-hosted mantle xenoliths started to occur early compared to world-wide where they are much more prevalent from the Cenozoic. The Glen Gollaidh and Clare Island (Upton et al. 2001) volcanics are the last mantle xenolith-hosting melts derived from small, volatile-rich melt-fractions before a change to a proliferation of large melt fraction (basaltic) melts. It is proposed that this point in the Devonian represents a time of significant change in the thickness, temperature or mechanical properties of continental lithosphere laterally allowing the large scale of fracturing required for penetration of basaltic melts.

Diamond prospectivity

The characteristics of the Glen Gollaidh aillikites of absence of definitively identified garnet grains, some relatively low Cr-content chromite and some spinel lherzolite Cr-diopside compositions are consistent with the failure of the sample tested to yield diamonds. The small sample size tested does not definitively prove that the body is non-diamondiferous but the negative result for both garnet and diamond makes the commercial prospects of the dyke itself very unlikely. While not derived from mantle thick enough to lie within the diamond stability field at this point, the Glen Gollaidh aillikite provides evidence for a craton margin with enough inferred thickness to suggest that it sits at the edge of diamond-prospective mantle lithosphere. Sufficient cratonic keel thickness to lie within the diamond stability field may occur only a short distance to the west. This may occur under the Lewisian west at Clare Island, Eire, as evidenced by spinel populations dominated by Mg chromite over Mg–Al chromite (Upton et al. 2001; the converse being the case at Glen Gollaidh). Certainly, if not under the Lewisian, then most likely the NAC keel lies within the diamond stability field under East Greenland. Currently East Greenland is not known as a diamond-bearing province, unlike its counterpart on West Greenland (e.g. Hutchison and Frei 2009) but it is very much under-explored.

In conclusion, study of the Glen Gollaidh aillikite considerably advances understanding of the limits of diamond prospective areas at the peripheries of the NAC, likely a relatively short distance to the north and west. Magmatism in the late Devonian was likely initiated as part of the dying stages of subduction of Avalonia below Laurentia as a consequence of slab break-off. Furthermore, the considerable variability of mantle geochemistry at Glen Gollaidh represents a microcosm of North Atlantic Craton evolution evidencing a complex multi-component system.

Acknowledgements Sample disaggregation was carried out by SelFrag AS and mineral separate and selection, and diamond testing by caustic fusion was conducted at the Saskatchewan Research Council. Mineral chemistry was determined at the School of GeoSciences, University of Edinburgh (major and minor elements) and the Australian National University's Research School of Earth Sciences (trace elements). Phlogopite separates were dated at the Scottish Universities Environmental Research Centre's Argon Isotope Facility, East Kilbride, UK. Deon DeBruin (Diamond Indicator Minerals Pty Ltd.; grain mount preparation), Chris Hayward (University of Edinburgh; EPMA), Hugh O'Neill, Greg Yaxley, Jung-Woo Park (Research School of Earth Sciences; La-ICP-MS support), Theo Ntaflos (University of Vienna, groundmass mineralogy), Wayne Taylor (Energy Metals Ltd.; La-ICP-MS standards and geochemical discussion), Alex Weh (SelFrag AS; sample fragmentation), Cristiana Mirceau (Saskatchewan Research Council; sample processing), and Heather Gow (site access) are all gratefully acknowledged. The manuscript benefitted from helpful reviews by Sonja Aulbach and Hugh O'Brien and from editorial handling by Graham Pearson and Lutz Nasdala.

References

Aulbach S, Viljoen KS (2015) Eclogite xenoliths from the Lace kimberlite, Kaapvaal craton: from convecting mantle source to palaeo-ocean floor and back. Earth Planet Sci Lett 431:274–286

Bernstein S, Hanghøj K, Kelemen PB, Brooks CK (2006) Ultra-depleted, shallow cratonic mantle beneath West Greenland: dunitic xenoliths from Ubekendt Ejland. Contrib Mineral Petrol 152:335–347

Bertrand P, Mercier J-CC (1985) The mutual solubility of coexisting ortho- and clinopyroxene: toward an absolute geothermometer for the natural system? Earth Planet Sci Lett 76:109–122

Bizzarro M, Stevenson RK (2003) Major element composition of the lithospheric mantle under the North Atlantic craton: evidence from peridotite xenoliths of the Sarfartoq area, southwestern Greenland. Contrib Mineral Petrol 146:223–240

Bonadiman C, Coltorti M, Duggen S, Paludetti L, Siena F, Thirlwall MF, Upton BGJ (2008) Palaeozoic subduction-related and kimberlite or carbonatite metasomatism in the Scottish lithospheric mantle. Geol Soc London Spec Publ 293:303–333

Chapman DS, Pollack HN (1977) Regional geotherms and lithospheric thickness. Geology 5:265–268

Dare SAS, Barnes S-J, Beaudoin G, Méric J, Boutroy E, Potvin-Doucet C (2014) Trace elements in magnetite as petrogenetic indicators. Mineral Deposita 49:785–796

Downes H, Upton BGJ, Connolly J, Beard AD, Bodinier J-L (2007) Petrology and geochemistry of a cumulate xenolith suite from

Bute: evidence for late Palaeozoic crustal underplating beneath SW Scotland. J Geol Soc Lond 164:1217–1231
Dziewonski AD, Anderson DL (1981) Preliminary reference Earth model. Phys Earth Planet Inter 25:297–356
Enfield MA, Coward MP (1987) The West Orkney Basin, northern Scotland. J Geol Soc Lond 144:871–884
Faithfull JW (2012) Gem sapphire and diamond potential in NW Scotland. Trans Inst Min Metall B 120:64
Goodenough KM, Millar I, Strachan RA, Krabbendam M, Evans JA (2011) Timing of regional deformation and development of the Moine Thrust Zone in the Scottish Caledonides: constraints from U–Pb geochronology of alkaline intrusions. J Geol Soc Lond 168: 99–144
Grütter HS (2009) Pyroxene xenocryst geotherms. Lithos 112S: 1167–1178
Grütter HS, Apter DB (1998) Kimberlite- and lamproite-borne chromite phenocrysts with "diamond inclusion"-type chemistries. 7th Int Kimberlite Conf Ext Abstr, pp 280–282
Grütter HS, Tuer J (2009) Constraints on deep mantle tenor of Sarfartoq-area kimberlites (Greenland), based on modern thermobarometry of mantle-derived xenocrysts. Lithos 112S:124–129
Grütter HS, Latti D, Menzies A (2006) Cr-saturation arrays in concentrate garnet compositions from kimberlite and their use in mantle barometry. J Petrol 47:801–820
Halliday AN, Stephens WE, Harmon RS (1980) Rb-Sr and O isotopic relationships in 3 zoned Caledonian granitic plutons, Southern Uplands, Scotland: evidence for varied sources and hybridisation of magmas. J Geol Soc Lond 137:329–348
Halliday AN, Aftalion M, Parsons I, Dickin AP, Johnson MRW (1987) Syn-orogenic alkaline magmatism and its relationship to the Moine Thrust Zone and the thermal state of the lithosphere in NW Scotland. J Geol Soc Lond 144:611–617
Hasterok D, Chapman DS (2011) Heat production and geotherms for the continental lithosphere. Earth Planet Sci Lett 307:59–70
Hollocher K, Ruiz J (1995) Major and trace element determinations on NIST glass standard reference materials 611, 612, 614, and 1834 by inductively coupled plasma-mas spectrometry. Geostand Newslett 19:27–34
Hughes JW (2012) The first reported occurrence of aillikite from the United Kingdom: potential for the GLSDP? Cardiff University, MESci thesis
Hughes HSR, McDonald I, Faithfull JW, Upton BGJ, Downes H (2015) Trace-element abundances in the shallow lithospheric mantle of the North Atlantic Craton margin: implications for melting and metasomatism beneath Northern Scotland. Mineral Mag 79:877–907
Hutchison MT (2011) Northern Territory diamond exploration database. Northern Territory Geol Surv Digit Inf Package DIP 011
Hutchison MT (2018) Data methodologies applied in the Western Australian diamond exploration package. Geol Surv West Aust Rec 2017(/16):24
Hutchison MT, Frei D (2009) Kimberlite and related rocks from Garnet Lake, West Greenland, including their mantle constituents, diamond occurrence, age and provenance. Lithos 112S:318–333
Kelley SP, Wartho J-A (2000) Rapid kimberlite ascent and the significance of Ar–Ar ages in xenolith phlogopites. Science 289:609–611
Kennedy C, Kennedy G (1976) The equilibrium boundary between graphite and diamond. J Geophys Res 81:2467–2470
Lancaster PJ, Strachan RA, Bullen D, Fowler M, Jaramillo M, Saldarriaga AM (2017) U–Pb zircon geochronology and geodynamic significance of 'Newer Granite' plutons in Shetland, northernmost Scottish Caledonides. J Geol Soc Lond 174:486–497
Macdonald R, Fettes DJ (2007) The tectonomagmatic evolution of Scotland. Trans Royal Soc Edinb Earth Sci 97:213–295
McDonough WF, Sun S-S (1995) The composition of the Earth. Chem Geol 120: 223–253
McKenzie D, Jackson J, Priestley K (2005) Thermal structure of oceanic and continental lithosphere. Earth Planet Sci Lett 233:337–349
Menzies MA, Halliday AN, Hunter RH, MacIntyre RM, Upton BJG (1989) The age, composition and significance of a xenolith-bearing monchiquite dike, Lewis, Scotland. Geol Soc Australia Spec Publ, vol 14. Blackwell Scientific Publications, Carlton, pp 843–852
Mitchell RH (1986) Kimberlites mineralogy, geochemistry and petrology. Plenum Press, New York, 442 p
Monaghan AA, Parrish RR (2006) Geochronology of Carboniferous-Permian magmatism in the Midland Valley of Scotland: implications for regional tectonomagmatic evolution and the numerical timescale. J Geol Soc Lond 163:15–28
Norman MD, Pearson NJ, Sharma A, Griffin WL (1996) Quantitative analysis of trace elements in geological materials by laser ablation ICPMS: instrumental operating conditions and calibration values of NIST glasses. Geostand Newslett 20:247–261
Phillips D (2012) Comment on "New Ar–Ar ages of southern Indian kimberlites and a lamproite and their geochemical evolution" by Osborne et al. [Precambrian Res. 189 (2011) 91–103]. Precambrian Res 208–211:49–52
Phillips D, Onstott TC (1988) Argon isotopic zoning in mantle phlogopite. Geology 16:542–546
Praegel N-O (1981) Origin of ultramafic inclusions and megacrysts in a monchiquite dyke at Streap, Inverness-shire, Scotland. Lithos 14: 305–322
Ramsay RR (1992) Geochemistry of diamond indicator minerals. Univ West Aust, Perth, Western Australia, PhD thesis (unpublished)
Ramsay RR, Tompkins LA (1994) The geology, heavy mineral concentrate mineralogy, and diamond prospectivity of the Boa Esperança and Cana Verde Pipes, Corrego D'Anta, Minas Gerais, Brazil. Companhia de Pesquisa de Recursos Minerais – CPRM Special Publication 1B Jan/94:329–345
Read HH (1931) The geology of central Sutherland (East-central Sutherland and south-western Caithness). Mem Geol Surv Scotl, Edinburgh, 238 p
Renne PR, Balco G, Ludwig KR, Mundil R, Min K (2011) Response to the comment by W.H. Schwarz et al. on "Joint determination of K-40 decay constants and Ar-40*/K-40 for the Fish Canyon sanidine standard, and improved accuracy for Ar-40/Ar-39 geochronology" by PR Renne, et al. (2010). Geochim Cosmochim Ac 75:5097–5100
Rock NMS (1986) The nature and origin of ultramafic lamprophyre, alnöite and related rocks. J Petrol 276:155–196
Smith CG, Faithfull JW, Jackson B (2008) Gemstone prospectivity in Scotland. In: Walton G (ed) The proceedings of the 14th Extractive Industry Conference. EIG Conferences, pp 9–11
Stephenson D (2000) Caledonian igneous rocks of Great Britain: an introduction. In: Stephenson D et al (eds) Caledonian Igneous Rocks of Great Britain, Geological Conservation Review Series, no, vol 17. Joint Nature Conservation Committee, Peterborough, pp 1–26
Stone P, Green PM, Lintern BC, Simpson PR, Plant JA (1993) Regional geochemical variation across the Iapetus Suture zone: tectonic implications. Scott J Geol 29:113–121
Sun S-S, McDonough WF (1989) Chemical and isotopic systematics of oceanic basalts: implications for mantle composition and processes. In: Saunders AD, Norry MJ (eds) Magmatism in the Ocean Basins, Geol Soc London Spec Publ, vol 42. Geol Soc London, London, pp 313–345
Tappe S, Foley SF, Jenner GA, Kjarsgaard BA (2005) Integrating ultramafic lamprophyres into the IUGS classification of igneous rocks: rationale and implications. J Petrol 46:1893–1900
Tappe S, Steenfelt A, Heaman LM, Simonetti A (2009) The newly discovered Jurassic Tikiusaaq carbonatite-aillikite occurrence, West Greenland, and some remarks on carbonatite–kimberlite relationships. Lithos 112S:385–399
Upton BGJ (2013) Tectono-magmatic evolution of the younger Gardar southern rift, South Greenland. Geol Surv Den Greenl Bull 29 124 p

Upton BGJ, Hinton RW, Aspen P, Finch A, Valley JW (1999) Megacrysts and associated xenoliths: evidence for migration of geochemically enriched melts in the Upper Mantle beneath Scotland. J Petrol 40: 935–956

Upton BGJ, Phillips WEA, Stillman CJ (2001) Late Paleozoic ultramafic magmatism on Clare Island, Co Ma. In: Graham JR (ed) New Survey of Clare Island, Geology, vol 2. Royal Irish Acad, Dublin, pp 63–74

Upton BGJ, Aspen P, Hinton RW (2003) Garnet pyroxenite xenoliths and pyropic megacrysts in Scottish alkali basalt. Scott J Geol 39:169–184

Upton BGJ, Stephenson D, Smedley PM, Wallis SM, Fitton JG (2004) Carboniferous and Permian magmatism in Scotland. In: Wilson S, Neuman E-R, Davies GR, Timmerman MJ, Heeremans M, Larsen BT (eds) Permo-Carboniferous magmatism and rifting in Europe, Geol Soc London Spec Publ, vol 223. Geol Soc London, London, pp 195–218

Upton BGJ, Craven JA, Kirstein LA (2006) Crystallisation of melaaillikites of the Narsaq region, Gardar alkaline province, south Greenland and relationships to other aillikitic–carbonatitic associations in the province. Lithos 92:300–319

Upton BGJ, Downes H, Kirstein LA, Bonadiman C, Hill PG, Ntaflos T (2011) The lithospheric mantle and lower crust–mantle relationships under Scotland: a xenolithic perspective. J Geol Soc Lond 168:873–885

Van Breeman O, Aftalion M, Johnson MR (1979) Age of the Loch Borrolan complex, assynt and late movements along the Moine Thrust Zone. J Geol Soc Lond 16:489–495

Wittig N, Webb M, Pearson DG, Dale CW, Ottley CJ, Hutchison M, Jensen SM, Luguet A (2010) Formation of the North Atlantic Craton: timing and mechanisms constrained from Re–Os isotope and PGE data of peridotite xenoliths from S.W. Greenland. Chem Geol 276:166–187

Yaxley G (2008) Technique for the discrimination of diamond indicator chromites from those of other provenance, based on major, minor and trace element analysis. Northern Territory Geological Survey, Open File Company Report CR2008–0177, Appendix 1, 15 p

Yaxley GM, Kamenetsky V (1999) In situ origin for glass in mantle xenoliths from southeastern Australia: insights from trace element compositions of glasses and metasomatic phases. Earth Planet Sci Lett 172:97–109